THE JOURNAL OF PHYSICAL CHEMISTRY LETTERS
A JOURNAL OF THE AMERICAN CHEMICAL SOCIETY

pubs.acs.org/JPCL

Letter

Entropic Stabilization of Water at Graphitic Interfaces

Tod A. Pascal* and William A. Goddard III

Cite This: J. Phys. Chem. Lett. 2021, 12, 9162−9168

Read Online

ACCESS | Metrics & More | Article Recommendations | Supporting Information

ABSTRACT: The thermodynamic stability of water next to graphitic surfaces is of fundamental interest, as it underlies several natural phenomena and important industrial processes. It is commonly assumed that water wets graphite more than graphene due to increased, favorable van der Waals interactions between the interfacial water molecules with multiple carbon sheets. Here, we employed extensive computer simulations and analysis of the molecular correlation functions to show that the interfacial water thermodynamics is in fact dominated by surface entropy. We show that on graphite, destabilization of the interfacial hydrogen bond network leads to an overcompensating increase in population of low frequency translational and librational modes, which is ultimately responsible for the increased interfacial stability compared to graphene. The spectroscopic signature of this effect is an enhancement of the modes near 100 and 300 cm^{-1}. This subtle interplay between entropy and surface binding may have important consideration for interpretations of various phenomena, including the hydrophobic effect.

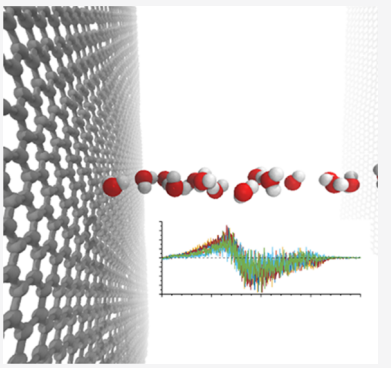

An understanding of the complex physics and chemistries of interfacial water is vital to understanding many natural phenomena[1,2] and for rational design strategies aimed at enhancing the performance of aqueous electrochemical systems.[3−6] Yet, the thermodynamic properties of water next to even simple interfaces remains the subject of much debate.[7−11] To this end, modern, powerful spectroscopic[12] and microscopy[13] techniques with very high resolution and surface sensitivity are being applied, but these measurements are frequently difficult to interpret. More traditional, macroscopic contact angle measurements are an indirect way of assessing the interfacial thermodynamics but are themselves hampered by the presence of surface impurities (e.g., absorbed small molecules) that lead to large uncertainties.[14]

Atomistic computer simulations, employing molecular dynamics (MD) and Monte Carlo techniques, are complementary tools that, in the current context, have been used to predict contact angles of nanodroplets of water on rigid graphene sheets. But these calculations are themselves limited by a fundamental length scale mismatch and the associated finite size effects.[15,16] We endeavor to rationalize the macroscopic behavior of systems from such microscopic simulations, *without* the need to apply empirical, Tolman-like[17] corrections. We thus consider a simple system: the solid/liquid free energy of water molecules between graphene sheets in a 2D periodic (infinite) geometry. A direct approach for calculating the relevant surface free energies has been frustrated in practice by the significant computational cost of exact approaches employing thermodynamic integration (TI). Additionally, while the free energy potential is a system observable, it would also be most useful to probe the role of local (i.e., distant dependent) solvent thermodynamics in informing overall stability. In this contribution, we employ an efficient approach to predict the absolute entropy and quantum corrections to the enthalpy of condensed phase simulations, based on analysis of the atomistic auto correlation functions over short, ∼20 ps MD simulations.[18,19] We then calculate the excess surface free energy of water molecules as a function of sheet thickness and distance from the interface, to elucidate the role of hydrogen bonding and correlated water dynamics in interfacial stability.

Figure 1a presents a schematic of our simulation setup, comprising a two-dimensional periodic box with 4353 water molecules encapsulated between 3.7 × 3.7 nm^2 graphene sheets of increasing thickness (Figure 1b). We describe the sheet−sheet interactions with the QMFF-Cx[20] force field, the water−water interactions primarily with the rigid TIP4P-2005[21] water model, and the water−carbon interactions using the empirical parameters of Werder and co-workers,[22] derived to reproduce an experimental contact angle of water on graphite of 84−86° in nanodroplet simulations. We focus here on the TIP4P-2005 water model due to its accuracy in reproducing the properties of the bulk liquid and the interfacial thermodynamics (specifically, the surface entropy) at the air−vapor interface.[23]

In agreement with previous MD simulations, we find the first interfacial water layer lies closer to graphite than to graphene

Received: August 9, 2021

https://doi.org/10.1021/acs.jpclett.1c02609
J. Phys. Chem. Lett. 2021, 12, 9162−9168

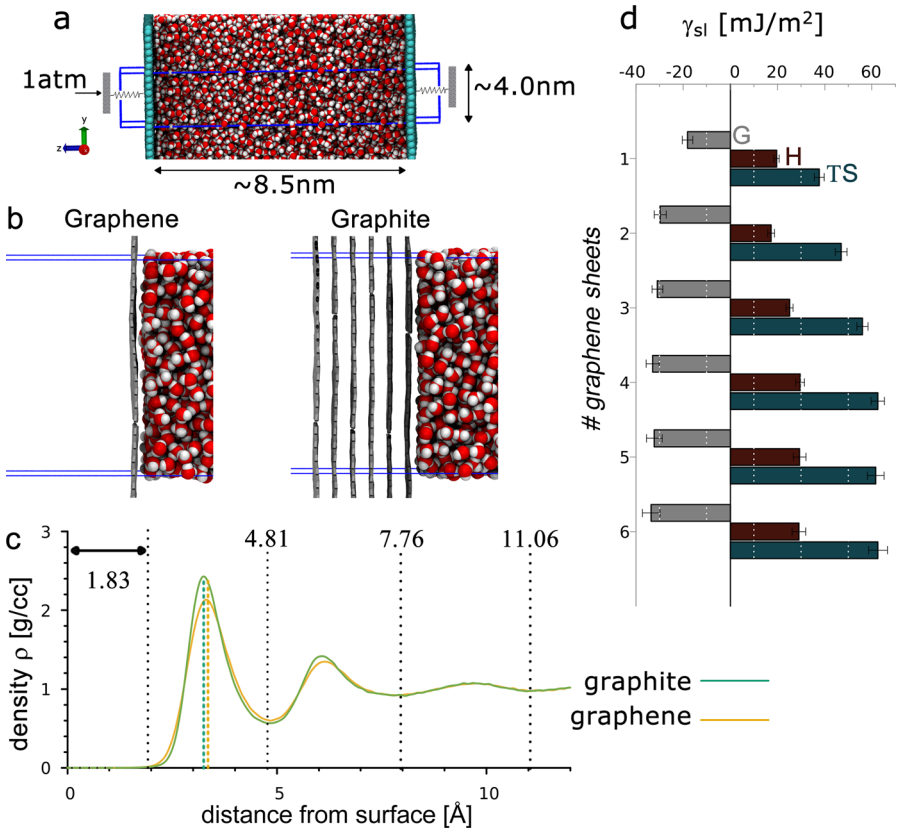

Figure 1. Interfacial thermodynamics. (a) Schematic of simulation cell (blue box) with 4353 water molecules encapsulated between parallel graphene sheets. (b) Final equilibrium MD snapshot of the top six layers of water on graphene (left) graphite (right). (c) Profile of water density away from the surface. Dotted vertical lines demarcate the water layers. Dashed lines indicate the position of the first peak maximum: 3.19 Å for graphite (yellow line) and 3.31 Å for graphene (green line). (d) Surface free energy (G − gray), enthalpy (H − red), and entropy (TS − green). Error bars are calculated uncertainty (standard deviation, 1σ).

and has a more asymmetric distribution. The mass density profiles in Figure 1c are obtained from the statistical average of the closest contact point between the center of mass of each water molecule and the instantaneous interface formed by the vibrating topmost sheet. We find characteristic density oscillations associated with a liquid next to a hard wall.[24]

On graphene, there are three distinguishable water layers:

- After an initial 1.8 Å exclusion zone, the first water layer extends up to 4.8 Å from the graphene surface, with a peak density of 2.1 g/cm^3 and an average distance of 3.32 Å.
- The second layer extends up to 7.7 Å with a peak density of 1.3 g/cm^3
- The third layer extends up to 11.0 Å with a peak density of 1.1 g/cm^3.

In contrast, the first water layer next to graphite lies closer to the surface, with an average distance of 3.25 Å (a ∼2% decrease) and a peak mass density of 2.4 g/cm^3 (a ∼14% increase). Moreover, we find that the first layer water distance distribution is more "normal" on graphene than on graphite: comparing to a normal distribution with the same variance, we find a smaller positive skewness (a third central moment of ∼0.27) and excess kurtosis (a fourth central moment of ∼1.89) than on graphite (0.52 and 2.05 respectively). Differences in the mass distribution persists in the second interfacial layer; however, we find no appreciable difference in properties of the third layer and beyond, which suggest a natural, sub-nanometer (∼8 Å) length scale for quantifying the interfacial thermodynamics.

The interfacial stability of water increases monotonically with graphene sheet thickness so that water on graphite has a lower surface free energy than on graphene. Figure 1d plots the excess surface free energy γ_{SL} of the water layer, relative to the bulk liquid: $\gamma_{SL}^{G} = \frac{\partial G}{\partial A} = c\frac{G_{system} - (G_{bulk\text{-}water} - G_{graphene\text{-}sheets})}{S.A.}$ where S.A. is the surface area (1370 Å^2) and c = 166.03 is a conversion factor to convert from kJ/mol/A^2 to mJ/m^2. Application of the TIP4P/2005 water model results in a calculated surface energy of water on graphene $\gamma_{SL}^{G} = -18.1 \pm 2.2$ mJ/m^2, corresponding to a work of adhesion $W_{SL} = \Delta\gamma = \gamma_{LV} - \gamma_{SL} = 82.5$ mJ/m^2, using the calculated liquid/vapor surface tension of 64.4 mJ/m^2. In comparison, the water surface free energy on bilayer graphene, $\gamma_{SL}^{G} = -29.7 \pm 2.5$ mJ/m^2, is significantly more favorable. We find that the surface free energy converges after four-layer graphene, so that for graphite $\gamma_{SL} = -33.5$ mJ/m^2, corresponding to a work of adhesion of $\Delta\gamma = 97.9$ mJ/m^2. The exact value for the work of adhesion of water on graphene/graphite is a dramatic function of the water model and water−carbon interaction potential and is actively being debated.[7,9,11,14,22,25−30] As a figure of merit, application of the SPC/E water model[31] results in a favorable $\gamma_{SL} = -30.6$ mJ/m^2 for water on graphene. This corresponds to a work of adhesion of $W_{SL} = 86.4$ mJ/m^2 using the calculated liquid/vapor surface tension $\gamma_{LV} = 55.8$ mJ/m^2, or 102.6 mJ/m^2 using the experimental surface tension $\gamma_{LV} = 72$ mJ/m^2, the latter in agreement with previous MD studies.[10,25] While the

https://doi.org/10.1021/acs.jpclett.1c02609
J. Phys. Chem. Lett. 2021, 12, 9162−9168

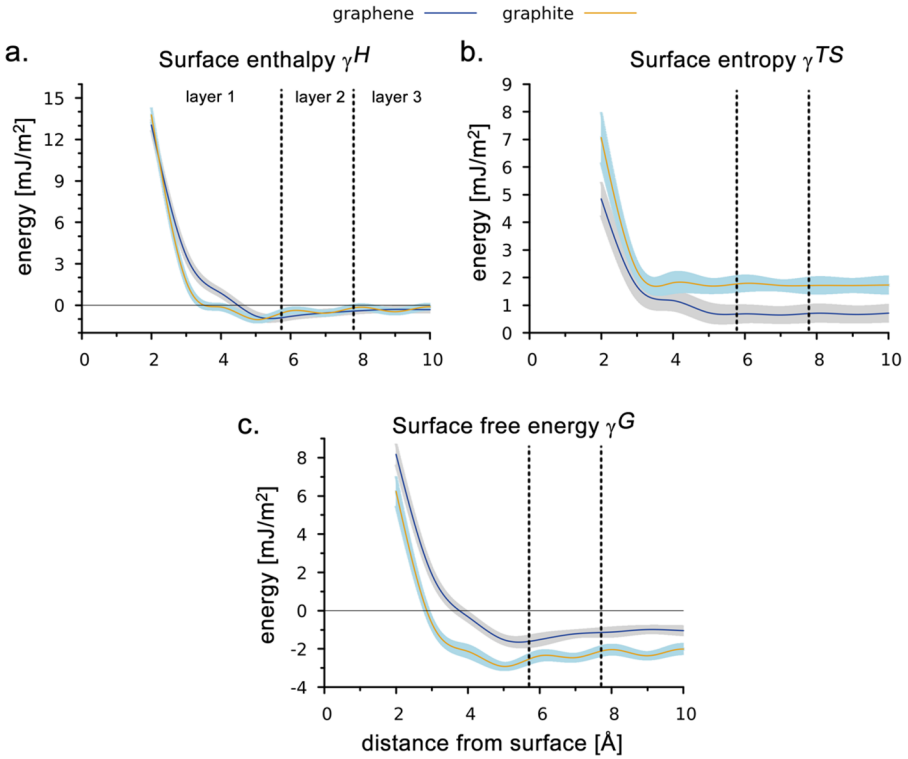

Figure 2. Stability of water layers on graphene and graphite. (a) Profile of the solid−liquid surface enthalpy $\gamma_{sL}{}^{H}$ of water on graphene (blue) and graphite (yellow) arising from specific water layers (denoted by dashed lines). The calculated data are connected with cubic splines to guide the eyes. The shaded region indicates the calculated uncertainty. (b) Surface entropy $\gamma_{sL}{}^{TS}$. (c) Surface free energy ($\gamma_{sL}{}^{G} = \gamma_{sL}{}^{H} - \gamma_{sL}{}^{TS}$).

calculated surface energies show some dependence on the water model or the water−carbon interaction potential employed, we note that the calculated difference in the solid/liquid surface energy $\gamma_{SL}{}^{\Delta G} = \gamma_{SL}{}^{G}$ (graphene) − $\gamma_{SL}{}^{G}$ (graphite) ranges from +12 to +19 mJ/m^2 (Tables S1 and S2). This suggests that our approach accurately captures the changing physics in water binding and dynamics with increased sheet thickness.

Figure 1d shows, perhaps surprisingly, that interfacial water molecules are enthalpically less stable on graphite than on graphene. Further insights are obtained by separately considering the contributions to the surface enthalpy arising from water−graphene sheet interactions (WG) and water−water interactions (WW) interactions. As shown in Table S3, the WG interactions increase monotonically with sheet thickness, as expected, due to increased surface binding (van der Waals - vdW) interactions. Thus, water molecules have an ∼9% stronger interaction energy with the carbon sheets in graphite, compared to graphene. The WW interactions, on the other hand, are significantly less favorable on graphite than on graphene. This arises from subtle changes in hydrogen bonding (H-bonding) of the first interfacial layer. In Figure S1, we present the normalized H-bonding profiles, which are non-monotonic and display oscillations similar to the mass density profile. Integrating over the first layer, we find an average of 2.67 ± 0.34 H-bonds/molecule on graphene (Figure S1c) or about ∼25% broken H-bonds. This is nearly twice the ∼14% broken H-bonds calculated in the bulk liquid, though significantly less than the ∼45% broken H-bonds calculated at the air−water interface.[23] In contrast, water molecules in the first interfacial layer on graphite have 2.47 ± 0.11 H-bonds/molecule. Thus, increased broken H-bonding dominates the more attractive vdW interactions so that the first layer is relatively destabilized on graphite compared to graphene.

Water molecules have higher entropy on graphite than on graphene, which overcompensates for the unfavorable enthalpy. The difference in entropy is the dominant term determining interfacial stability. Indeed, while the relative surface enthalpy $\gamma_{SL}{}^{\Delta H} = -9.5 \pm 3.1$ mJ/m^2 favors graphene, the relative surface entropy $\gamma_{SL}{}^{\Delta S} = -24.9 \pm 7.2$ mJ/m^2 greatly favors graphite, which overall leads to the relative surface free energy $\gamma_{SL}{}^{\Delta G} = 15.5$ mJ/m^2 and increased water stability on graphite.

Further insights are obtained from considering the thermodynamic signature of the various water layers (Figure S2). Our approach for calculating the thermodynamics relies solely on the atomic velocities, which provides a natural way to decompose the total system thermodynamics into contributions arising from water layers, defined from the mass density profile in Figure 1. We find that the interfacial enthalpies are primarily encoded in the H-bonding of the first interfacial water layer, accounting for 92% of the total in graphene and 73% in graphite (Figure 2a, Table S5). The entropy function, on the other hand, shows relatively long tails on graphite (Figure 2b). First consider that on graphene, each molecule in the first interfacial layer gains on average $T\Delta S = 0.8 \pm 0.1$ kJ/mol of total energy compared to the bulk (an increase of ∼4.4%), stabilizing the surface by $\gamma_{SL}{}^{TS} = 13.6 \pm 0.5$ mJ/m^2, or 36% of the total. In comparison, on graphite, the first layer water molecules gain even more entropy, with $T\Delta S = 1.1 \pm 0.7$ kJ/mol, a ∼ 6.1% increase. This corresponds to $\gamma_{SL}{}^{TS} = 18.5 \pm 0.3$ mJ/m^2 of entropic stability, representing ∼30% of the total. Moreover, on graphene, we find convergence to the bulk after the fourth interfacial layer. On graphite, the excess entropy function decays much more slowly so that the water molecules

https://doi.org/10.1021/acs.jpclett.1c02609
J. Phys. Chem. Lett. 2021, 12, 9162−9168

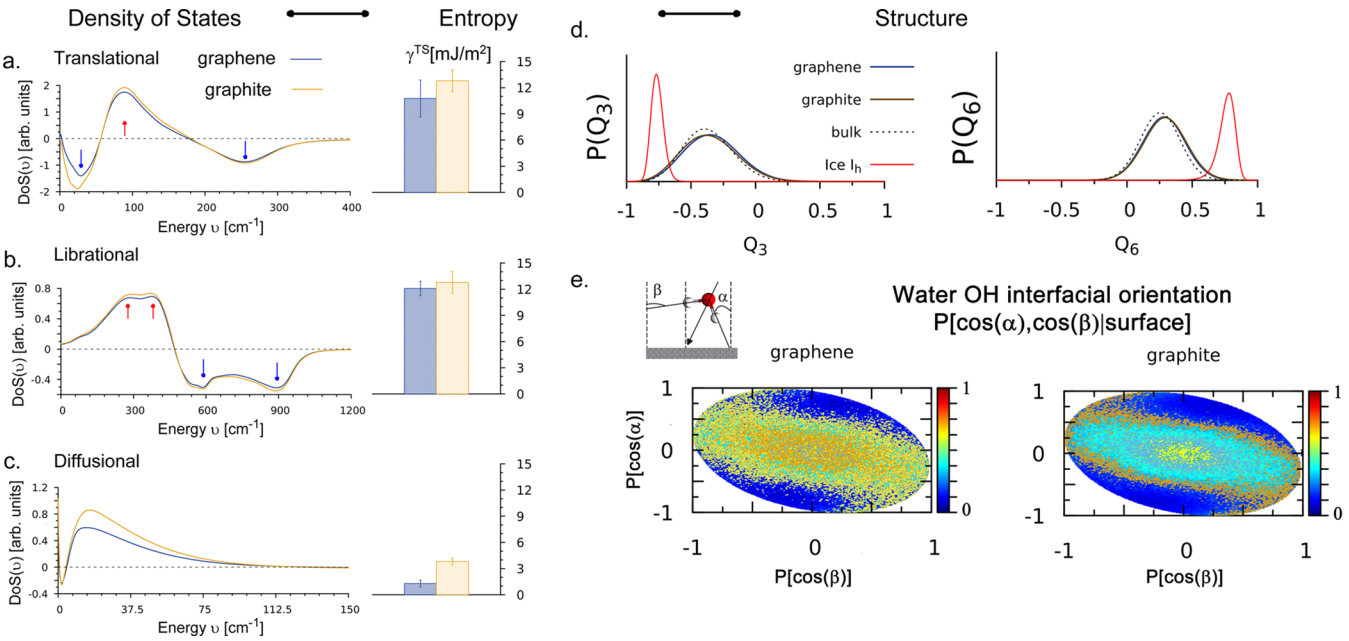

Figure 3. Spectroscopy at aqueous graphitic interfaces. (a) Differential diffusional density of states (DoS) of the first interfacial water layer on graphene (blue) and graphite (brown) relative to bulk water. (Right inset) Excess solid−liquid entropy obtained by considering only the diffusional water modes. (b) Translational DoS resulting from low frequency rattling motions (as in a solid). (c) Rotational modes DoS. (d) Probability distribution of globally averaged bond-orientational order parameters Q_3 (left) and Q_6 (right) for the first interfacial water layer on graphene and graphite. Distributions for bulk water (dashed black line) and hexagonal ice (simulated at 200 K − red line) are given as a reference. There is no signature of icelike motifs at the graphitic interfaces. (e) Normalized joint conditional probability distribution of the OH vector−surface normal angles cos(α) and cos(β) (left inset), describing the orientation of a water molecules in the surface layer relative to the bulk. Redder shades indicate higher probabilities. Maximum probabilities lies near cos(α,β) = 0 of molecules lying flat on the surface.

in the seventh interfacial layer (∼2.3 nm away from the surface) lower the interfacial energy by γ_{SL}^{TS} = 2.1 ± 0.2 mJ/m^2. In fact, our calculations indicate that convergence of the entropy to the bulk value is not achieved until the 12th interfacial layer on graphite, ∼4 nm from the surface.

Interfacial water molecules next to graphitic interfaces have a unique spectroscopic signature, distinct from the bulk. We quantify this by means of the density of states (DOS − spectral density or power) spectrum. As demonstrated in Figure 3, we further separate the total surface entropy γ_{SL}^{TS} of the first two interfacial layers on graphene and graphite into three components: $\gamma_{SL}^{TS} = \gamma_{SL}^{TS\text{-translational}} + \gamma_{SL}^{TS\text{-librational}} + \gamma_{SL}^{TS\text{-diffuse}}$ for the center of mass translations (Figure 3a), librational (rotational) (Figure 3b), and diffusional (Figure 3c) contributions, respectively. Note that we consider molecular motions associated with low frequency rattling motions (as in a solid) as the translational entropy, as distinct from the more usual configurational entropy, which includes the librational (rotational) motions; i.e., $\gamma_{SL}^{TS\text{-conf}} = \gamma_{SL}^{TS\text{-libration}}\ \gamma_{SL}^{TS\text{-translations}}$.

The dominant factor acting to lower the interfacial surface free energy is enhanced translational entropy, accounting for 22.1 mJ/m^2 (60% of the total) of entropic stabilization for water on graphene and 53.0 mJ/m^2 (86% of the total) on graphite. Spectroscopically, this manifests as an enhancement of the low frequency rattling modes from 85−125 cm^{-1}, and the appearance of a new peak in the spectrum near 100 cm^{-1} (Figure 3a). Here, the effect is more pronounced on graphite than on graphene due to weakened H-bonding on graphite due to the increased water density. Moreover, we also find that the translational entropic enhancement on graphite has a surprisingly long spatial decay length (Figure S3) and is responsible for the entropy function not decaying until the seventh interfacial layer.

Enhanced librational entropy (Figure 3b) of interfacial water next to graphitic interfaces is the other significant entropic stabilization, leading to an enhancement of states around 300 and 350 cm^{-1}, with a corresponding depopulation of the rotational states around 600 and 900 cm^{-1}. In the bulk, rotations are highly quantized due to the tetrahedral hydrogen bonding and proceed collectively through a "jump reorientational" mechanism.[32,33] At the interface, broken hydrogen bonding apparently facilitates populations of these other, lower energy, rotational states. We calculate that that enhanced rotational dynamics in the first two interfacial layers contribute γ_{SL}^{TS} = +12.8 mJ/m^2 and +12.0 + = 0.8 mJ/m^2 for graphite and graphene, respectively.

Water molecules in the first two interfacial layers have enhanced diffusion compared to the bulk, with a calculated self-diffusion constant of 2.65 and 2.91 cm^2/s for graphene and graphite respectively, compared to the bulk water value of 2.35 ± 0.13 cm^2/s. It has been established that, for 2D systems, there is a large anisotropy in the self-diffusion constant, with the in-plane being enhanced, while the out-of-plane is suppressed.[34] Indeed, our calculated in-plane self-diffusion constant was found to be 2.5 times larger than the out-of-plane value. Spectroscopically, this manifest as an enhancement of the DoS at zero frequency (Figure 3c). The distribution of diffusive modes is also generally enhanced, primarily due to the increase of the in-plane self-diffusion noted previously: we calculate that the percentage of purely diffusive modes increases to 23.7% and 24.6% at the graphene and graphite interfaces respectively, compared to 22.8 ± 0.6% in the bulk liquid. Overall, we calculate an increase in the relative

https://doi.org/10.1021/acs.jpclett.1c02609
J. Phys. Chem. Lett. 2021, 12, 9162−9168

diffusional entropy for water at graphitic interfaces, which stabilizes the interface by lowering the surface free energy by $\gamma_{SL}^{TS\text{-diffuse}}$ = +1.4 and +5.2 mJ/m^2 (3.7% and 8.3% of the total), respectively.

A fourth component of the molecular motions involves the internal vibrations of the water molecules (O−H bond stretching and H−O−H angle bending) and their effect on interfacial stability. Of course, TIP4P/2005 is a rigid water model that fixes the internal degrees of freedom. Thus, to consider these internal vibrations, we performed an additional set of calculations using the associated, flexible TIP4P/2005f[35] model. Overall, this results in slightly more negative surface energies but importantly shows similar trends in the surface thermodynamics with increasing sheet thickness: namely, an entropy-dominated stabilization of water on graphite compared to graphene. We find that the first layer water molecules at either graphitic surfaces have an extra peak in the IR-active stretching modes around 3660 cm^{-1} (Figure S4) characteristic of "free" OH stretching.[36] We also find an overall blue-shift of ∼25 cm^{-1} of the main O−H stretching peak near 3600 cm^{-1}, which we predict should be visible to surface-sensitive probes such as surface enhanced infrared spectroscopy. The relatively high frequencies of these vibrational modes means that they contribute relatively little to the increased surface entropy (<0.004 mJ/m^2). However, these modes contribute significantly to the zero-point energy, which presents a significant isotope effect for nanoconfined geometries.[37]

Our translational and librational entropy results are consistent with previous predictions of the stabilization of water molecules in carbon nanotubes.[38] In both cases, the results contrast sharply with expectations of the "iceberg" model,[39] which posits that that water molecules near a hydrophobic solute are icelike and immobilized. Indeed, we show in Figure 3d, by means of the Q_3 and Q_6 Steinhardt bond-order parameters,[40,41] that there is no evidence of icelike molecules at these graphitic interfaces. Further evidence is obtained from considering the relative orientation of the water molecules near the interface, from the joint probability distribution function of the two OH bond vectors. As shown in Figure 3e, the orientation where the plane defined by the water molecule atoms lies parallel to the graphene surface is preferred. The distribution is not sufficiently sharply peaked to indicate immobilization but rather is fairly broad, especially on graphite. Moreover, this weak orientational effect mostly vanishes by the third interfacial layer (Figure S5).

Finally, it is important to consider the molecular origin of the relatively long tails of the entropy potential on graphite, compared to graphene. These arise primarily from the modification of the water−water fluctuations in the first interfacial layer. Here, by increasing the population of low energy translational and librational states, water molecules on graphite increase their overall entropy. Concomitantly, these low energy, long wavelength states propagate further from the surface. Although different in focus, our results are consistent with the modification of long-range dipolar fluctuations (in some cases up to 10s of nanometers) for water molecules next to model hydrophobic interfaces, reported both experimentally[42] and computationally.[43]

In summary, we have demonstrated by means of extensive computer simulations that the major driving force for the increased stability of water molecules on graphite compared to graphene is the water surface entropy and increased population of low energy states in the first few interfacial water layers. Thus, interfacial entropic forces communicate through the graphene sheet and affect water dynamics, an effect that could be opposite and, in some cases, overcompensates for changes in interfacial binding energy. Moreover, we show that the entropy function has a surprisingly long tail, with water layers almost 4 nm away from the surface contributing to the surface energy. This may have important consequences for adsorption of ions and small molecules at the graphite interface, where the temperature-dependent populations and binding free energies may differ significantly from that of graphene. This could in turn impact the performance and function of aqueous devices, such as graphene-based supercapacitors, due to subtle changes in the electric double layer(s). Our results also suggest significant nanoscale "confinement effects"[37,44−49] in simulation cells comprising water molecules between parallel graphene/graphite sheets. In particular, below the 4 nm convergence lengths, the entropy function will be significantly modified, and the zero-point energy effect may dominate interfacial thermodynamics. This was recently demonstrated experimentally by surface force apparatus experiments and by computer simulations.[37] Future studies will employ more sophisticated approaches to describe the intermolecular interactions, including the explicit consideration of many-body polarization effects,[50] which have been shown previously to significantly affect the interfacial entropy of water on graphene.[25]

■ ASSOCIATED CONTENT

Supporting Information

The Supporting Information is available free of charge at https://pubs.acs.org/doi/10.1021/acs.jpclett.1c02609.

Extensive computational methods, Tables S1−S5 showing the various energies and Figures S1−S5 showing the H-bonding profiles and other thermodynamic potentials (PDF)

■ AUTHOR INFORMATION

Corresponding Author

Tod A. Pascal − *ATLAS Materials Physics Laboratory, Department of NanoEngineering and Chemical Engineering and Materials Science and Engineering, University of California San Diego, La Jolla, California 92093, United States;* orcid.org/0000-0003-2096-1143; Email: tpascal@ucsd.edu

Author

William A. Goddard III − *Materials and Process Simulation Center, California Institute of Technology, Pasadena, California 91125, United States;* orcid.org/0000-0003-0097-5716

Complete contact information is available at: https://pubs.acs.org/10.1021/acs.jpclett.1c02609

Notes

The authors declare no competing financial interest.

■ ACKNOWLEDGMENTS

This work was initiated with funds from Dow Chemical Corporation (Willie Lau and Joe Rokowski) and NSF (CBET-1067848, George Antos). It was completed with funding from NSF (CBET-1805022, Robert McCabe Pgm Mgr.) (W.A.G.) and funding from NSF (T.A.P.) through the UC San Diego

Materials Research Science and Engineering Center (UCSD MRSEC), DMR-2011924. T.A.P. acknowledges the start-up fund from the Jacob School of Engineering at the University of California, San Diego (UCSD). Portions of this work was completed as a user project at the Molecular Foundry, a U.S. Department of Energy Nanoscience Facility at Lawrence Berkeley National Laboratory supported by the Office of Science, Office of Basic Energy Sciences, of the U.S. DOE under Contract No. DE-AC02-05CH11231. Some simulations used resources of the National Energy Research Scientific Computing Center, specifically allocation m3047, which is supported by the Office of Science of the U.S. Department of Energy under the same contract. This work also used the Extreme Science and Engineering Discovery Environment (XSEDE) and the CSD626 allocation on the Comet supercomputer at the San Diego Supercomputing Center, which is supported by National Science Foundation Grant Number ACI-1548562.

REFERENCES

(1) DeMott, P.; Chen, Y.; Kreidenweis, S.; Rogers, D.; Sherman, D. E. Ice formation by black carbon particles. *Geophys. Res. Lett.* **1999**, *26* (16), 2429−2432.
(2) Charlson, R. J.; Seinfeld, J. H.; Nenes, A.; Kulmala, M.; Laaksonen, A.; Facchini, M. C. Reshaping the theory of cloud formation. *Science* **2001**, *292* (5524), 2025−2026.
(3) Liu, C.; Yu, Z.; Neff, D.; Zhamu, A.; Jang, B. Z. Graphene-based supercapacitor with an ultrahigh energy density. *Nano Lett.* **2010**, *10* (12), 4863−4868.
(4) Wang, Y.; Shi, Z.; Huang, Y.; Ma, Y.; Wang, C.; Chen, M.; Chen, Y. Supercapacitor devices based on graphene materials. *J. Phys. Chem. C* **2009**, *113* (30), 13103.
(5) Qu, L.; Liu, Y.; Baek, J.-B.; Dai, L. Nitrogen-doped graphene as efficient metal-free electrocatalyst for oxygen reduction in fuel cells. *ACS Nano* **2010**, *4* (3), 1321−1326.
(6) Nair, R.; Wu, H.; Jayaram, P.; Grigorieva, I.; Geim, A. Unimpeded permeation of water through helium-leak-tight graphene-based membranes. *Science* **2012**, *335* (6067), 442−444.
(7) Rafiee, J.; Mi, X.; Gullapalli, H.; Thomas, A. V.; Yavari, F.; Shi, Y.; Ajayan, P. M.; Koratkar, N. A. Wetting transparency of graphene. *Nat. Mater.* **2012**, *11* (3), 217−222.
(8) Li, Z.; Wang, Y.; Kozbial, A.; Shenoy, G.; Zhou, F.; McGinley, R.; Ireland, P.; Morganstein, B.; Kunkel, A.; Surwade, S. P.; Li, L.; Liu, H. Effect of airborne contaminants on the wettability of supported graphene and graphite. *Nat. Mater.* **2013**, *12* (10), 925−931.
(9) Shih, C.-J.; Wang, Q. H.; Lin, S.; Park, K.-C.; Jin, Z.; Strano, M. S.; Blankschtein, D. Breakdown in the wetting transparency of graphene. *Phys. Rev. Lett.* **2012**, *109* (17), 176101.
(10) Taherian, F.; Marcon, V.; van der Vegt, N. F.; Leroy, F. D. R. What is the contact angle of water on graphene? *Langmuir* **2013**, *29* (5), 1457−1465.
(11) Shih, C.-J.; Strano, M. S.; Blankschtein, D. Wetting translucency of graphene. *Nat. Mater.* **2013**, *12* (10), 866−869.
(12) Velasco-Velez, J.-J.; Wu, C. H.; Pascal, T. A.; Wan, L. F.; Guo, J.; Prendergast, D.; Salmeron, M. The structure of interfacial water on gold electrodes studied by x-ray absorption spectroscopy. *Science* **2014**, *346* (6211), 831−834.
(13) Xu, K.; Cao, P.; Heath, J. R. Graphene visualizes the first water adlayers on mica at ambient conditions. *Science* **2010**, *329* (5996), 1188−1191.
(14) Xu, K.; Heath, J. R. Wetting: Contact with what? *Nat. Mater.* **2013**, *12* (10), 872−873.
(15) Checco, A.; Guenoun, P.; Daillant, J. Nonlinear dependence of the contact angle of nanodroplets on contact line curvature. *Phys. Rev. Lett.* **2003**, *91* (18), 186101.
(16) Bresme, F.; Quirke, N. Computer simulation study of the wetting behavior and line tensions of nanometer size particulates at a liquid-vapor interface. *Phys. Rev. Lett.* **1998**, *80* (17), 3791.
(17) Tolman, R. C. Consideration of the Gibbs theory of surface tension. *J. Chem. Phys.* **1948**, *16* (8), 758−774.
(18) Lin, S.-T.; Maiti, P. K.; Goddard, W. A. Two-Phase Thermodynamic Model for Efficient and Accurate Absolute Entropy of Water from Molecular Dynamics Simulations. *J. Phys. Chem. B* **2010**, *114* (24), 8191−8198.
(19) Desjarlais, M. P. First-principles calculation of entropy for liquid metals. *Phys. Rev. E* **2013**, *88* (6), 062145.
(20) Pascal, T. A.; Karasawa, N.; Goddard, W. A., III Quantum mechanics based force field for carbon (QMFF-Cx) validated to reproduce the mechanical and thermodynamics properties of graphite. *J. Chem. Phys.* **2010**, *133* (13), 134114.
(21) Abascal, J. L.; Vega, C. A general purpose model for the condensed phases of water: TIP4P/2005. *J. Chem. Phys.* **2005**, *123* (23), 234505.
(22) Werder, T.; Walther, J. H.; Jaffe, R.; Halicioglu, T.; Koumoutsakos, P. On the water-carbon interaction for use in molecular dynamics simulations of graphite and carbon nanotubes. *J. Phys. Chem. B* **2003**, *107* (6), 1345−1352.
(23) Pascal, T. A.; Goddard, W. A., III Interfacial Thermodynamics of Water and Six Other Liquid Solvents. *J. Phys. Chem. B* **2014**, *118* (22), 5943−5956.
(24) Allen, M. P.; Tildesley, D. J. *Computer Simulation of Liquids*; Oxford University Press, 2017.
(25) Misra, R. P.; Blankschtein, D. Insights on the role of many-body polarization effects in the wetting of graphitic surfaces by water. *J. Phys. Chem. C* **2017**, *121* (50), 28166−28179.
(26) Raj, R.; Maroo, S. C.; Wang, E. N. Wettability of graphene. *Nano Lett.* **2013**, *13* (4), 1509−1515.
(27) Fowkes, F. M.; Harkins, W. D. The state of monolayers adsorbed at the interface solid—aqueous solution. *J. Am. Chem. Soc.* **1940**, *62* (12), 3377−3386.
(28) van Engers, C. D.; Cousens, N. E.; Babenko, V.; Britton, J.; Zappone, B.; Grobert, N.; Perkin, S. Direct measurement of the surface energy of graphene. *Nano Lett.* **2017**, *17* (6), 3815−3821.
(29) Dutta, R. C.; Khan, S.; Singh, J. K. Wetting transition of water on graphite and boron-nitride surfaces: A molecular dynamics study. *Fluid Phase Equilib.* **2011**, *302* (1−2), 310−315.
(30) Jaffe, R. L.; Gonnet, P.; Werder, T.; Walther, J. H.; Koumoutsakos, P. Water-carbon interactions 2: calibration of potentials using contact angle data for different interaction models. *Mol. Simul.* **2004**, *30* (4), 205−216.
(31) Berendsen, H. J. C.; Grigera, J. R.; Straatsma, T. P. The missing term in effective pair potentials. *J. Phys. Chem.* **1987**, *91* (24), 6269−6271.
(32) Asbury, J. B.; Steinel, T.; Kwak, K.; Corcelli, S.; Lawrence, C.; Skinner, J.; Fayer, M. Dynamics of water probed with vibrational echo correlation spectroscopy. *J. Chem. Phys.* **2004**, *121* (24), 12431−12446.
(33) Laage, D.; Hynes, J. T. A molecular jump mechanism of water reorientation. *Science* **2006**, *311* (5762), 832−835.
(34) Zhang, Y.; de Aguiar, H. B.; Hynes, J. T.; Laage, D. Water structure, dynamics, and sum-frequency generation spectra at electrified graphene interfaces. *J. Phys. Chem. Lett.* **2020**, *11* (3), 624−631.
(35) González, M. A.; Abascal, J. L. F. A flexible model for water based on TIP4P/2005. *J. Chem. Phys.* **2011**, *135* (22), 224516.
(36) Scatena, L.; Brown, M.; Richmond, G. Water at hydrophobic surfaces: weak hydrogen bonding and strong orientation effects. *Science* **2001**, *292* (5518), 908−912.
(37) Shrestha, B. R.; Pillai, S.; Santana, A.; Donaldson, S. H., Jr; Pascal, T. A.; Mishra, H. Nuclear Quantum Effects in Hydrophobic Nanoconfinement. *J. Phys. Chem. Lett.* **2019**, *10* (18), 5530−5535.
(38) Pascal, T. A.; Goddard, W. A.; Jung, Y. Entropy and the driving force for the filling of carbon nanotubes with water. *Proc. Natl. Acad. Sci. U. S. A.* **2011**, *108* (29), 11794−11798.

https://doi.org/10.1021/acs.jpclett.1c02609
J. Phys. Chem. Lett. 2021, 12, 9162−9168

(39) Frank, H. S.; Evans, M. W. Free Volume and Entropy in Condensed Systems III. Entropy in Binary Liquid Mixtures; Partial Molal Entropy in Dilute Solutions; Structure and Thermodynamics in Aqueous Electrolytes. *J. Chem. Phys.* **1945**, *13* (11), 507−532.
(40) Steinhardt, P. J.; Nelson, D. R.; Ronchetti, M. Bond-orientational order in liquids and glasses. *Phys. Rev. B: Condens. Matter Mater. Phys.* **1983**, *28* (2), 784.
(41) Rein ten Wolde, P.; Ruiz-Montero, M. J.; Frenkel, D. Numerical calculation of the rate of crystal nucleation in a Lennard-Jones system at moderate undercooling. *J. Chem. Phys.* **1996**, *104* (24), 9932−9947.
(42) Tielrooij, K.; Paparo, D.; Piatkowski, L.; Bakker, H.; Bonn, M. Dielectric relaxation dynamics of water in model membranes probed by terahertz spectroscopy. *Biophys. J.* **2009**, *97* (9), 2484−2492.
(43) Zhang, C.; Gygi, F.; Galli, G. Strongly anisotropic dielectric relaxation of water at the nanoscale. *J. Phys. Chem. Lett.* **2013**, *4* (15), 2477−2481.
(44) Fumagalli, L.; Esfandiar, A.; Fabregas, R.; Hu, S.; Ares, P.; Janardanan, A.; Yang, Q.; Radha, B.; Taniguchi, T.; Watanabe, K.; Gomila, G.; Novoselov, K. S.; Geim, A. K. Anomalously low dielectric constant of confined water. *Science* **2018**, *360* (6395), 1339−1342.
(45) Senapati, S.; Chandra, A. Dielectric Constant of Water Confined in a Nanocavity. *J. Phys. Chem. B* **2001**, *105* (22), 5106−5109.
(46) Ruiz-Barragan, S.; Muñoz-Santiburcio, D.; Körning, S.; Marx, D. Quantifying anisotropic dielectric response properties of nano-confined water within graphene slit pores. *Phys. Chem. Chem. Phys.* **2020**, *22* (19), 10833−10837.
(47) Motevaselian, M. H.; Aluru, N. R. Universal Reduction in Dielectric Response of Confined Fluids. *ACS Nano* **2020**, *14* (10), 12761−12770.
(48) Schlaich, A.; Knapp, E. W.; Netz, R. R. Water Dielectric Effects in Planar Confinement. *Phys. Rev. Lett.* **2016**, *117* (4), 048001.
(49) Olivieri, J.-F.; Hynes, J. T.; Laage, D. Confined Water's Dielectric Constant Reduction Is Due to the Surrounding Low Dielectric Media and Not to Interfacial Molecular Ordering. *J. Phys. Chem. Lett.* **2021**, *12*, 4319−4326.
(50) Naserifar, S.; Goddard, W. A., III *J. Chem. Phys.* **2018**, *149* (17), 174502.

https://doi.org/10.1021/acs.jpclett.1c02609
J. Phys. Chem. Lett. 2021, 12, 9162−9168